Temporal dynamics of strongly coupled epsilon near-zero plasmonic systems Ⓕ

Mehdi H. Ebrahim, Andrea Marini, Vincenzo Bruno, et al.

COLLECTIONS

Note: This paper is part of the APL Special Collection on Zero-index Metamaterials for Classical and Quantum Light.

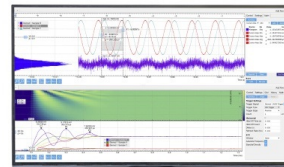Ⓕ   This paper was selected as Featured

View Online   **Export Citation**   **CrossMark**

Temporal dynamics of strongly coupled epsilon near-zero plasmonic systems ⓕ

Mehdi H. Ebrahim,[1] Andrea Marini,[2] Vincenzo Bruno,[3] Nathaniel Kinsey,[4] ⓘD Jacob B. Khurgin,[5] ⓘD Daniele Faccio,[3] ⓘD and Matteo Clerici[1,a)] ⓘD

AFFILIATIONS

[1]James Watt School of Engineering, University of Glasgow, G12 8QQ Glasgow, United Kingdom
[2]Department of Physical and Chemical Sciences, University of L'Aquila, Via Vetoio, 67100 L'Aquila, Italy
[3]School of Physics and Astronomy, University of Glasgow, G12 8QQ Glasgow, United Kingdom
[4]Department of Electrical and Computer Engineering, Virginia Commonwealth University, Richmond, Virginia 23284, USA
[5]Department of Electrical and Computer Engineering, Johns Hopkins University, Baltimore, Maryland 21218, USA

Note: This paper is part of the APL Special Collection on Zero-index Metamaterials for Classical and Quantum Light.
[a)]Author to whom correspondence should be addressed: matteo.clerici@glasgow.ac.uk

ABSTRACT

Subwavelength epsilon-near-zero (ENZ) films with decorated nanoantennae are an emerging platform for coupling radiation into the ENZ mode: recent experiments have shown how strong coupling between the two systems underpins significant nonlinear effects. Field enhancement and the temporal dynamic of the radiation in ENZ films strongly coupled with plasmonic antennae play a substantial role in the light–matter interaction, and the latter has not yet been fully disclosed. We numerically investigate the pulse shaping of radiation impinging on two representative strongly coupled systems: a transparent conductive oxide with ENZ in the NIR band (ITO) and a polar material with ENZ in the MIR (SiC). In both cases, we demonstrate that the temporal dynamics and field enhancement are particularly pronounced within the strong coupling region, and we highlight the different polarization responses of the ITO-based case from the SiC one. The latter, owing to lower losses, shows extreme reshaping of resonant radiation close to the ENZ spectral region and is, therefore, a promising candidate for slow-light-enhanced effects.

Published under an exclusive license by AIP Publishing. https://doi.org/10.1063/5.0070296

The epsilon near-zero (ENZ) mode arising in deeply subwavelength ENZ films is tightly confined and field-enhanced due to the continuity of the longitudinal component of the electric field,[1] the large group index of the bulk material, and the slow-light effect consequent of the flat modal dispersion.[2–5] Such conditions underpin increased optical nonlinear effects,[6–10] e.g., enhanced harmonic generation,[1,11–14] a giant Kerr effect,[15–17] strong negative refraction, and high efficiency of four-wave mixing (FWM).[18,19] Unfortunately, the ENZ mode is not easily accessible from free space due to its large impedance mismatch with the radiation in air.[20] Among the strategies devised to overcome this issue, one approach exploits the hybridization of the ENZ mode with plasmonic antennas deposited on top of the ENZ film[21–24] and shows strongly enhanced nonlinearities.[18,25] In this regime of the light–matter interaction, field enhancement and slow-light both contribute to increasing the nonlinear effects. The antennae-ENZ-substrate metasurfaces (MSs) have been predominantly investigated with indium-tin oxide (ITO) as the ENZ layer, and the enhanced light–matter interactions have been linked to slow-light effects increasing the interaction time between light and matter.[9] While field enhancement can be numerically assessed with finite-difference time-domain (FDTD) simulations by analyzing the spectrum of a broadband source, unveiling the temporal dynamics requires a time-resolved analysis of the FDTD simulated radiation dynamics, which has not been fully addressed yet.

Here, we fill this gap by investigating the temporal dynamics driven by the pulsed excitation of a strongly coupled system comprised of plasmonic antennae and an ENZ film. We have considered two representative ENZ media, namely, a transparent conductive oxide (TCO) with an ENZ frequency in the near-infrared, $\nu_{\mathrm{ENZ}} = 211$ THz (ITO, $\lambda_{\mathrm{ENZ}} = 1420$ nm) and a polar dielectric (silicon carbide, SiC) with a longitudinal optical phonon resonance in the mid-infrared at $\lambda_{\mathrm{LO}} = 10.3\ \mu$m. In the latter case, the phonon resonance is responsible for a low-loss ENZ condition at $\nu_{\mathrm{ENZ}} = 29.1$ THz. The frequency-dependent permittivities for the two media are shown in Figs. S1(a) and S1(b) of the supplementary material.

Our numerical analysis shows that the strong coupling condition enables to increase the pulse duration and delay. These effects are particularly evident for the normal and in-plane field components at higher and lower frequency resonances. Our results show that losses play a major role in quenching both the duration and the delay of the enhanced field inside the ENZ medium. SiC, featuring losses three orders of magnitudes smaller than those of TCOs[26] ($\gamma_{ITO} \geq 1.5 \times 10^{14}$ rad s^{-1}, $\gamma_{SiC} \geq 9.4 \times 10^{11}$ rad s^{-1}, see the supplementary material), is, therefore, a promising solution for slow-light applications.[27]

Strong-coupling (SC) is relevant in nanophotonics as it enables fine-tuning of the system response to external stimuli: A tiny variation of the system characteristics produces, indeed, large qualitative modifications of its response. It arises from the hybridization and anti-crossing of two distinct resonant excitations, which can be thought of as coupled harmonic oscillators. To model the SC system, it is possible to consider the simple case of two classical harmonic oscillators, with resonant angular frequencies ω_e, ω_p and dissipation rates γ_e, γ_p

coupled by the coupling strength Ω—see Fig. 1(a). In this case, the eigenfrequencies ν_+, ν_- of the system supermodes follow:[28]

$$\nu_\pm = \frac{1}{2\pi}\left[\tilde{\omega} \pm \frac{\Delta}{2}\sqrt{1 + \left(\frac{2\Omega}{\Delta}\right)^2}\right], \quad (1)$$

where

$$\tilde{\omega} = \frac{\omega_e + \omega_p}{2} - i\frac{\gamma_e + \gamma_p}{4} \quad (2)$$

$$\Delta = \omega_e - \omega_p - i\frac{\gamma_e - \gamma_p}{2}. \quad (3)$$

The onset of strong coupling is identified by the transition from a perturbative to non-perturbative solution to the system dynamics, which occurs for $R_{SC} = |2\Omega/\Delta| \geq 1$,[28] where $\tilde{\omega}$ and Δ are the average complex frequency of the bare states and their complex detuning,
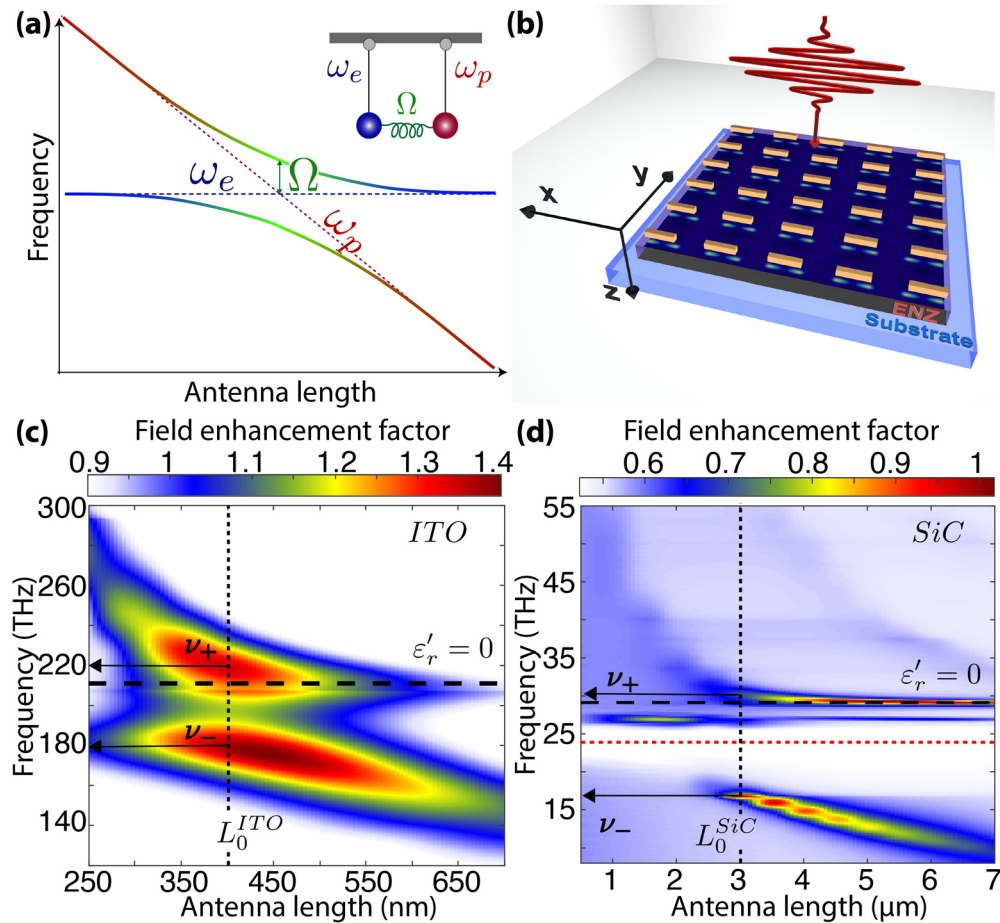

FIG. 1. (a) Anticrossing and SC-induced dispersion resulting from two classical harmonic oscillators with resonant frequencies ω_e and ω_p coupled by a strength Ω. (b) Sketch of a Au/ENZ/Substrate metasurface undergoing strong-coupling resonant excitation: the light blue and gray regions indicate the substrate and the ENZ layer (we considered ITO and SiC), respectively. The latter is decorated by a periodic array of gold-based nano-antennas (Au). [(c) and (d)] Field enhancement $|E/E_0|^2$ dependence over the impinging carrier frequency and antenna length for (c) ITO- and (d) SiC-based ENZ thin film of thicknesses $t_{ITO} = 20$ nm and $t_{SiC} = 150$ nm, respectively. The dashed black horizontal lines mark the ENZ frequencies of the two materials. The red dotted line in (d) shows the transverse optical phonon polariton resonance $\nu_{TO} = \omega_{TO}/2\pi$ of SiC. The region with a negative real part of the permittivity ε', between ν_{TO} and the ENZ frequency—ν_{LO}, is the Reststrahlen band. Finally, the vertical black dotted lines indicate the antenna lengths of maximal SC strength L_0.

respectively. Solutions where the real and imaginary part of the two eigenvalues of the coupled system Hamiltonian coalesce ($\omega_e = \omega_p$ and $|\gamma_e - \gamma_p| = 4\Omega$) are known as exceptional points, which mark the boundary between strong and weak coupling.[28,29] We tested the strong coupling condition for both the investigated systems (antennae for the ITO and SiC ENZ films). To that end, we first characterized the resonances ω_e and ω_p and dissipation rates γ_e and γ_p of the individual components as described in the supplementary material. In a second step, we numerically simulated the hybridization of the ENZ mode (a bulk plasmon in ITO and a collective LO phonon excitation in the SiC) with the nanoantennae cavity resonances (Au array decorated on top of films). We simulate the Au/ENZ/substrate MS shown in Fig. 1(b) for varying antennae lengths (L) and using a broadband approach and a commercial FDTD software (Lumerical). To this end, we injected a short, 6.6 fs for the ITO case and 33 fs for SiC, pulse into the simulation box and analyzed the spectrum of the electric field. The antennae with w and thickness d were kept constant to $w = 110$ nm, $d = 30$ nm for the ITO, and $w = 250$ nm, $d = 40$ nm for the SiC MSs. The simulations are performed with periodic boundary conditions on the transverse spatial directions, and the box size is chosen in such a way to avoid antenna–antenna coupling effects. The numerical results

shown in Figs. 1(c) and 1(d) allowed us to establish the frequencies of the strongly coupled systems ν_+ and ν_-. Combining these with the previous results allowed us to determine the strong coupling parameter $R_{SC} = |2\Omega/\Delta|$ and the antenna length at which the coupling is maximized. We obtained $R_{ITO} = 1.37$ at $L_0 = 400$ nm and $R_{SiC} = 1.28$ at $L_0 = 3\,\mu$m, which confirmed that both systems are strongly coupled at those antenna lengths.

Another metric used to assess the SC regime is given by the ratio between the energy exchange rate and the overall loss rates:[30] $R = 2\Omega/(\gamma_e + \gamma_p)$ (see Ref. 28 for a discussion on the different definitions of SC). $R > 1$ indicates that the resonances of the coupled system are visible. Based on the numerical simulations described above, we obtained $R_{ITO} = 2.42$ and $R_{SiC} = 3.20$.

We note that, by tuning the antenna length, it is not only possible to manipulate the excitation frequency, but also the field distribution within the MS. Indeed, while the ENZ mode, at angular frequency ω_e in Fig. 1(a), is polarized normal to the film plane (field directed along the z-direction), the antenna cavity mode (at angular frequency ω_p) is mainly polarized along the in-plane transverse direction.

Figure 2 shows how the antenna length influences the relative weight of the electric field polarization components $|E_x/E_M|$ [(a) and
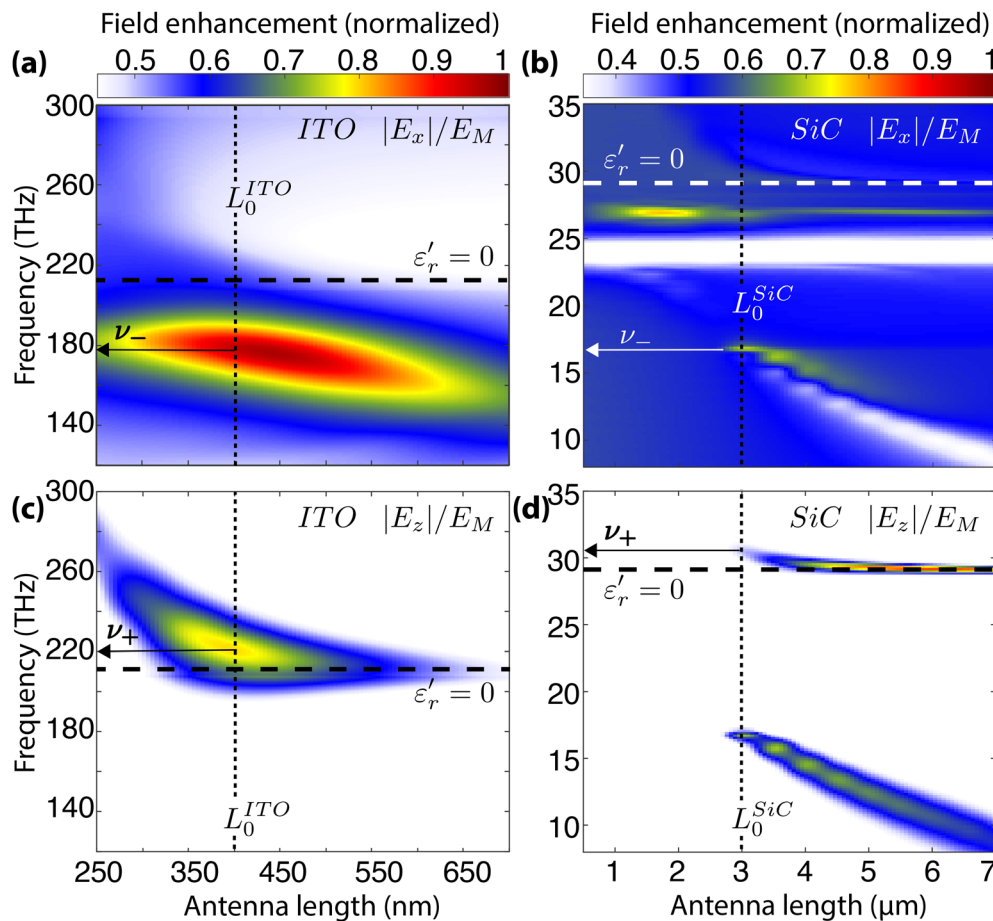

FIG. 2. Dependence of the relative enhancements of the spatially averaged field components $|E_x/E_M|$ [(a) and (b)] and $|E_z/E_M|$ [(c) and (d)] on the excitation frequency and the antenna length for the [(a) and (c)] ITO- and [(b) and (d)] SiC-based MSs illustrated in Fig. 1.

(b)] and $|E_z/E_M|$ for both the ITO- (a) and (c) and SiC-based (b) and (d) MSs. Here, E_M is the maximum field amplitude for the selected component within the structure. It should be noted that the input pulse is polarized in-plane (along the antenna length, x-direction). Therefore, while SC removes the distinction between antenna and ENZ modes, it is interesting to note that the higher frequency resonance (ν_+) is almost entirely z-polarized, thus exhibiting ENZ-mode behavior. In turn, the lower frequency mode (ν_-) is mainly transverse polarized and is, therefore, antenna-like. This is not as evident, however, with the SiC-based MS, as shown in Figs. 2(b) and 2(d). Here, similarly to the ITO case, we do not observe a transverse polarized ν_+ resonance. However, an additional "pinned," transverse polarized, enhanced field component appears close to the ENZ frequency, at around 27 THz. In contrast to the ITO case, the field component normal to the film is enhanced at both ν_+ and ν_-, with a "pinned" resonance at the ENZ frequency. We note that this behavior is a consequence of the SiC optical phonon polariton resonance $\nu_{TO} = \omega_{TO}/2\pi = 23.9$ THz appearing in the gap between ν_+ and ν_-. Radiation is coupled to the transverse optical phonons either by hybridization of the polaritonic modes consequence of the spatial localization, or by the plasmonic resonances of the metallic

antenna.[31,32] Numerical simulations performed in a dispersion landscape similar to that of SiC, but with ν_{TO} artificially shifted at frequencies far smaller than ν_- led to the disappearance of the observed pinned resonance. Furthermore, artificially increasing the losses of such a system to values similar to that of ITO leads to results similar to what was observed in the ITO case.

A similar pattern can also be observed exploring the spatial properties of the enhanced radiation. For the ITO MS, it is indeed clear that the two resonances ν_+ and ν_- have ENZ-mode- and antenna-like behaviors. Figure S3 in the supplementary material shows indeed how ν_- is localized at the antenna edges (and is polarized in-plane). At the same time, ν_+, mainly polarized in the direction normal to the film, expands into the ITO below the antenna. For the SiC MS, instead, ν_+ and ν_- have both antenna- and ENZ-mode-like behaviors.

ENZ materials have large group velocity dispersion and are known to slow radiation and reshape the temporal profile, allowing the impinging pulse to persist inside the medium for far longer than its input duration.[2] In turn, the considered SC regime enables the manipulation of the system dispersion and the effective radiation coupling into the ENZ material. To investigate the radiation dynamics mediated by the metasurface, we performed FDTD simulations with a
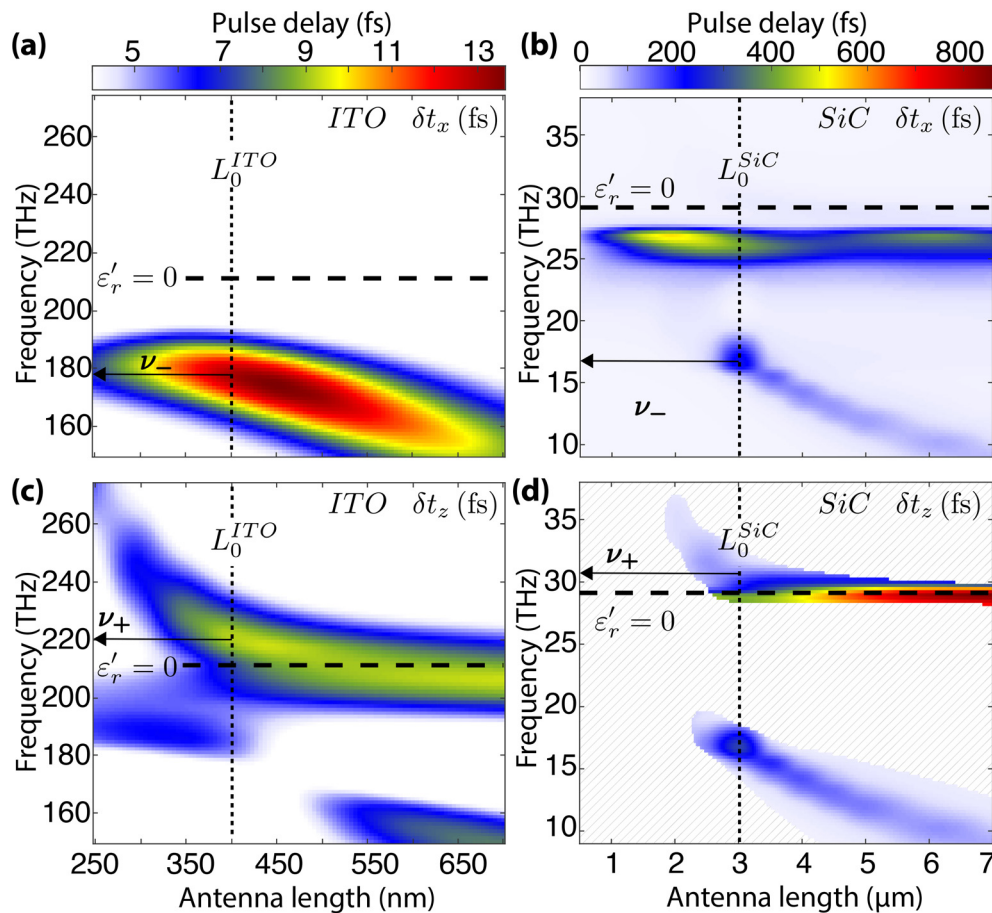

FIG. 3. Dependence of the group delay (in fs) of the [(a) and (b)] $|E_x|$ and [(c) and (d)] $|E_z|$ field components on the excitation frequency and the antenna length for the [(a) and (c)] ITO- and [(b) and (d)] SiC-based MSs.

commercial software (Lumerical) for impinging ultrafast pulses with in-plane polarization (field directed along the x-direction, i.e., along the antenna length), carrier frequency ν_0 ranging from 14 to 300 THz and pulse duration $\tau = 0.05$ and 0.5 ps for the ITO and SiC, respectively. Differently from the previous numerical simulations, here we have analyzed the temporal properties of the radiation into the sample, rather than its spectrum, and at varying carrier frequencies. This way, we characterized the dependence of the radiation dynamics from the different resonant and coupling conditions. We analyzed the temporal dynamics at the resonances of the system focusing on the delay $\delta t = t_{out} - t_{in}$, where $t_{in,out}$ is the pulse energy density center of mass (COM) at the input and output, respectively, and on the pulse duration change $\Delta t = \Delta t_{out} - \Delta t_{in}$. These quantities are shown in Figs. 3 and 4, respectively. The fields are measured at the longitudinal coordinate (z) corresponding to the interface between the ENZ film and the substrate and at the transverse coordinate (y) corresponding to the edge of the antenna.

As expected, similar to what was observed for the field enhancement (Fig. 2) both the delay δt (Fig. 3) and the pulse duration Δt (Fig. 4) depend on the excited mode (polarization) and have maxima in the region where SC occurs. For ITO, Figs. 3(a) and 3(c), the delay

incurred crossing the 20 nm film peaks at the ν_- and ν_+ resonances, for the antenna-like (a) and the ENZ-like (c) mode, respectively. The maximum recorded delay of $\simeq 13$ fs occurs for the antenna-like excitation and corresponds to an energy velocity index of $n_u \simeq 85$, measured considering the pulse COM. In contrast, for the ENZ-like mode, the energy velocity index is $n_u \simeq 20$. The situation is similar, although less straightforward, for the SiC MS—Figs. 3(b) and 3(d). In this case, the strong dispersion occurring when approaching the TO phonon resonance ($\lambda_{TO} = 12.55\,\mu m$) introduces further contributions to the temporal dynamics. For this reason, the delay and pulse duration computed for the SiC MS have only been plotted for $|E_z/E_M| > 0.2$ [the striped areas in Figs. 3(d) and 4(d) identify those regions where $|E_z/E_M| \leq 0.2$]. Large delays can be observed for the z-polarized field component field component in proximity to the system resonances ν_+ and ν_-, see Fig. 3(d). In contrast, no significant delay is observed for the x field component at ν_+, see Fig. 3(b). The low losses of SiC result in a significantly higher group index and higher Q-factor. In particular, the "pinned" mode exhibits a strong slow-light effect, similar to what was observed for the field enhancement.
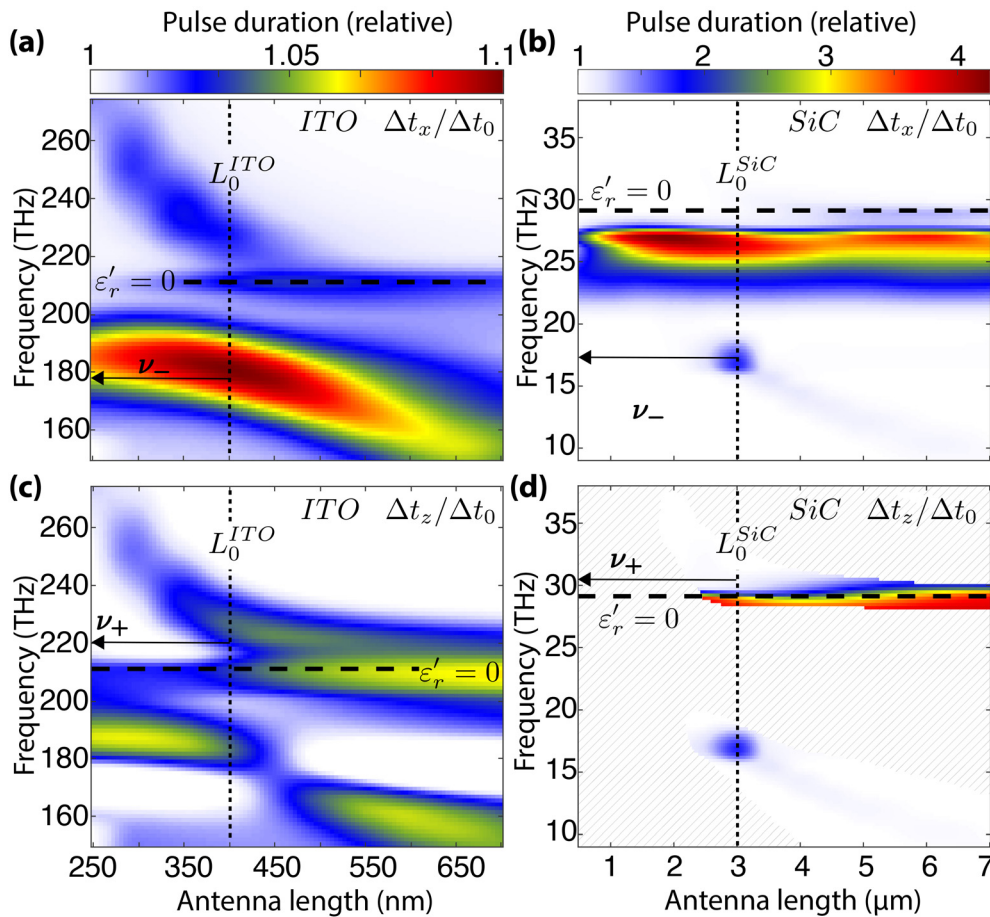

FIG. 4. Dependence of the pulse duration (relative to the input pulse duration) of the [(a) and (b)] $|E_x|$ and [(c) and (d)] $|E_z|$ field components on the excitation frequency and the antenna length for the [(a) and (c)] ITO- and [(b) and (d)] SiC-based MSs.
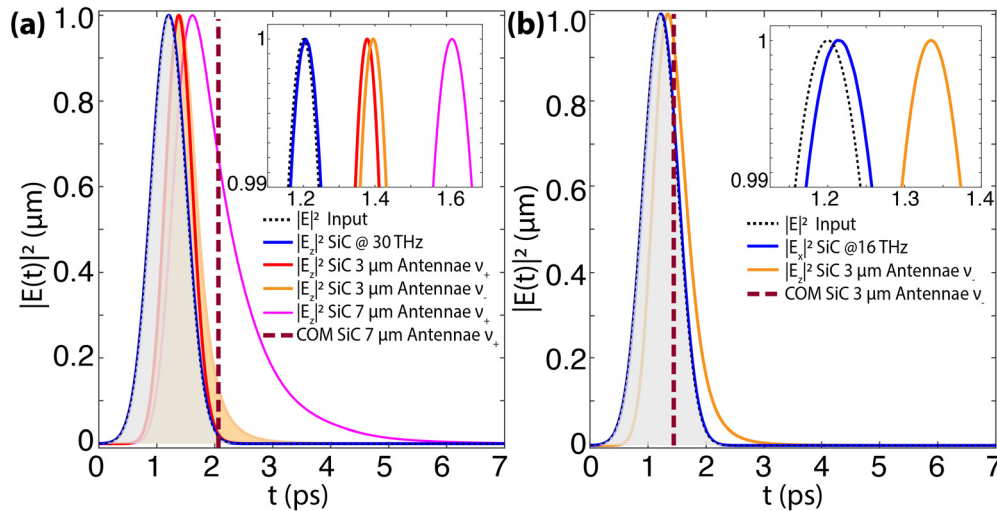
FIG. 5. Pulse envelopes in SiC. (a) The envelope corresponding to the z component of the field for the conditions where it is maximally delayed. The black dashed (and shaded) curve is the input pulse envelope (polarized in the x-direction), and the blue curve is the output pulse in the absence of the nanoantennae. The red and orange curves are the pulses after propagating through the 150 nm thick SiC sample patterned with the 3 μm long antennae, at ν_+, ν_- carrier frequencies, respectively. The magenta curve is the pulse at the ENZ frequency after propagating through the 150 nm thick SiC sample patterned with the 7 μm long antennae. The vertical thick dashed line indicates the COM of this latter pulse. (b) The envelope corresponding to the transverse (x) component of the electric field oscillating at the ν_- excitation and for the 3 μm-long antennae. The two insets show a detail of the pulse peaks and serve the purpose to visually compare the pulse delayed at the system's resonant excitations with what could be expected in the case of propagating through an unpatterned SiC sample of the same thickness (blue curves).

The strong curvature of the dispersion relations characterizing the radiation shown in Figs. 1(c) and 1(d) indicates that large group velocity dispersion effects are expected at the SC condition. The numerical simulations performed with pulsed inputs and shown in Fig. 4 confirm this expectation. The pulse duration changes significantly and increases more than fourfold for the SiC MS—Figs. 4(b) and 4(d). A similar effect is observed with ITO, albeit with a more modest 1.1× increase in the pulse duration—Figs. 4(a) and 4(c).

Representative examples of the temporal effects for the SiC MS are shown in Fig. 5. For a 29 THz carrier frequency pulse impinging on a MS with 7 μm-long antennae, we observed a remarkable maximum delay of $\delta t \simeq 860$ fs of the z field component COM, corresponding to $n_u \simeq 1700$, see Fig. 5(a). Notably, these are also the antennae length and excitation conditions that correspond to the maximal expected field enhancement, see Figs. 2(d) and 1(d). Significant delays are also recorded at the system resonances $\nu_+ \simeq 30$ THz and $\nu_- \simeq 16.6$ THz for the SC system with antennae length $L_0 \simeq 3 \mu$m. For such a MS, we obtained $\delta t_{-,x} \simeq 237$ fs ($n_u \simeq 473$); $\delta t_{-,z} \simeq 195$ fs ($n_u \simeq 389$); $\delta t_{+,z} \simeq 188$ fs ($n_u \simeq 376$). The pulse profiles for these conditions are shown in Fig. 5.

In conclusion, we have shown that the sustained energy transfer between the electromagnetic wave and a collective oscillation of electrons (ITO) and optical phonons (SiC) arising in strongly coupled antennae/ENZ systems leads to significant pulse reshaping. In both cases, the material excitation is localized on the timescale of the driving optical pulse, leading to a delay of the scattered electromagnetic wave. The longer delays observed with SiC are a consequence of the longer lifetime of the LO phonons. The investigated ENZ-based MSs are an alluring platform for manipulating the temporal pulse properties at the nanoscale, with a complex interplay between field enhancement and slow-light effects that may underpin a rich nonlinear phenomenology. Owing to the expected low losses and large delays, SiC-based MSs may play a significant role in future linear and nonlinear pulse shaping applications.

See the supplementary material for the strong-coupling model and numerical results. In addition, it proposes numerical results for the spatial and spatial-spectral field enhancement.

AUTHOR DECLARATIONS

Conflict of Interest

The authors have no conflicts to disclose.

DATA AVAILABILITY

All the data supporting the conclusions reported in this manuscript are available at the DOI:10.5525/gla.researchdata.1198.

REFERENCES

[1]M. A. Vincenti, D. de Ceglia, A. Ciattoni, and M. Scalora, "Singularity-driven second- and third-harmonic generation at ϵ-near-zero crossing points," Phys. Rev. A **84**, 063826 (2011).

[2]A. Ciattoni, A. Marini, C. Rizza, M. Scalora, and F. Biancalana, "Polariton excitation in epsilon-near-zero slabs: Transient trapping of slow light," Phys. Rev. A **87**, 053853 (2013).

[3]A. Ciattoni, C. Rizza, A. Marini, A. D. Falco, D. Faccio, and M. Scalora, "Enhanced nonlinear effects in pulse propagation through epsilon-near-zero media," Laser Photonics Rev. **10**, 517–525 (2016).

[4]M. H. Javani and M. I. Stockman, "Real and Imaginary Properties of Epsilon-Near-Zero Materials," Phys. Rev. Lett. **117**, 107404 (2016).

[5]J. B. Khurgin, M. Clerici, V. Bruno, L. Caspani, C. DeVault, J. Kim, A. Shaltout, A. Boltasseva, V. M. Shalaev, M. Ferrera *et al.*, "Adiabatic frequency shifting in epsilon-near-zero materials: The role of group velocity," Optica **7**, 226–231 (2020).

[6]A. Ciattoni, C. Rizza, and E. Palange, "Extreme nonlinear electrodynamics in metamaterials with very small linear dielectric permittivity," Phys. Rev. A **81**, 043839 (2010).

[7]C. Argyropoulos, P.-Y. Chen, G. D'Aguanno, N. Engheta, and A. Alù, "Boosting optical nonlinearities in ϵ-near-zero plasmonic channels," Phys. Rev. B **85**, 045129 (2012).

[8]I. Liberal and N. Engheta, "Near-zero refractive index photonics," Nat. Photonics **11**, 149–158 (2017).

[9]O. Reshef, I. De Leon, M. Z. Alam, and R. W. Boyd, "Nonlinear optical effects in epsilon-near-zero media," Nat. Rev. Mater. **4**, 535 (2019).

[10]N. Kinsey, C. DeVault, A. Boltasseva, and V. M. Shalaev, "Near-zero-index materials for photonics," Nat. Rev. Mater. **4**, 742–760 (2019).

[11]T. S. Luk, D. de Ceglia, S. Liu, G. A. Keeler, R. P. Prasankumar, M. A. Vincenti, M. Scalora, M. B. Sinclair, and S. Campione, "Enhanced third harmonic generation from the epsilon-near-zero modes of ultrathin films," Appl. Phys. Lett. **106**, 151103 (2015).

[12]A. Capretti, Y. Wang, N. Engheta, and L. D. Negro, "Enhanced third-harmonic generation in si-compatible epsilon-near-zero indium tin oxide nanolayers," Opt. Lett. **40**, 1500–1503 (2015).

[13]N. C. Passler, I. Razdolski, D. S. Katzer, D. F. Storm, J. D. Caldwell, M. Wolf, and A. Paarmann, "Second harmonic generation from phononic epsilon-near-zero berreman modes in ultrathin polar crystal films," ACS Photonics **6**, 1365–1371 (2019).

[14]Y. Yang, J. Lu, A. Manjavacas, T. S. Luk, H. Liu, K. Kelley, J.-P. Maria, E. L. Runnerstrom, M. B. Sinclair, S. Ghimire, and I. Brener, "High-harmonic generation from an epsilon-near-zero material," Nat. Phys. **15**, 1022–1026 (2019).

[15]N. Kinsey, C. DeVault, J. Kim, M. Ferrera, V. M. Shalaev, and A. Boltasseva, "Epsilon-near-zero al-doped zno for ultrafast switching at telecom wavelengths," Optica **2**, 616–622 (2015).

[16]M. Z. Alam, I. D. Leon, and R. W. Boyd, "Large optical nonlinearity of indium tin oxide in its epsilon-near-zero region," Science **352**, 795–797 (2016).

[17]L. Caspani, R. Kaipurath, M. Clerici, M. Ferrera, T. Roger, J. Kim, N. Kinsey, M. Pietrzyk, A. D. Falco, V. M. Shalaev *et al.*, "Enhanced nonlinear refractive index in ε-near-zero materials," Phys. Rev. Lett. **116**, 233901 (2016).

[18]V. Bruno, C. DeVault, S. Vezzoli, Z. Kudyshev, T. Huq, S. Mignuzzi, A. Jacassi, S. Saha, Y. Shah, S. Maier *et al.*, "Negative refraction in time-varying strongly coupled plasmonic-antenna–epsilon-near-zero systems," Phys. Rev. Lett. **124**, 043902 (2020).

[19]V. Bruno, S. Vezzoli, C. DeVault, E. Carnemolla, M. Ferrera, A. Boltasseva, V. M. Shalaev, D. Faccio, and M. Clerici, "Broad frequency shift of parametric processes in epsilon-near-zero time-varying media," Appl. Sci. **10**, 1318 (2020).

[20]S. Campione, I. Brener, and F. Marquier, "Theory of epsilon-near-zero modes in ultrathin films," Phys. Rev. B **91**, 121408 (2015).

[21]Y. C. Jun, J. Reno, T. Ribaudo, E. Shaner, J.-J. Greffet, S. Vassant, F. Marquier, M. Sinclair, and I. Brener, "Epsilon-near-zero strong coupling in metamaterial-semiconductor hybrid structures," Nano Lett. **13**, 5391–5396 (2013).

[22]S. A. Schulz, A. A. Tahir, M. Z. Alam, J. Upham, I. D. Leon, and R. W. Boyd, "Optical response of dipole antennas on an epsilon-near-zero substrate," Phys. Rev. A **93**, 063846 (2016).

[23]S. Campione, J. R. Wendt, G. A. Keeler, and T. S. Luk, "Near-infrared strong coupling between metamaterials and epsilon-near-zero modes in degenerately doped semiconductor nanolayers," ACS Photonics **3**, 293–297 (2016).

[24]N. C. Passler, C. R. Gubbin, T. G. Folland, I. Razdolski, D. S. Katzer, D. F. Storm, M. Wolf, S. De Liberato, J. D. Caldwell, and A. Paarmann, "Strong coupling of epsilon-near-zero phonon polaritons in polar dielectric heterostructures," Nano Lett. **18**, 4285–4292 (2018).

[25]M. Z. Alam, S. A. Schulz, J. Upham, I. D. Leon, and R. W. Boyd, "Large optical nonlinearity of nanoantennas coupled to an epsilon-near-zero material," Nat. Photonics **12**, 79–83 (2018).

[26]J. B. Khurgin, "How to deal with the loss in plasmonics and metamaterials," Nat. Nanotechnol. **10**, 2–6 (2015).

[27]Y. Li, I. Liberal, and N. Engheta, "Structural dispersion–based reduction of loss in epsilon-near-zero and surface plasmon polariton waves," Sci. Adv. **5**, eaav3764 (2019).

[28]S. R.-K. Rodriguez, "Classical and quantum distinctions between weak and strong coupling," Eur. J. Phys. **37**, 025802 (2016).

[29]ŞK. Özdemir, S. Rotter, F. Nori, and L. Yang, "Parity–time symmetry and exceptional points in photonics," Nat. Mater. **18**, 783–798 (2019).

[30]L. Novotny, "Strong coupling, energy splitting, and level crossings: A classical perspective," Am. J. Phys. **78**, 1199–1202 (2010).

[31]B. K. Ridley, *Electrons and Phonons in Semiconductor Multilayers* (Cambridge University Press, 2014).

[32]J. Chen and J. B. Khurgin, "Optical phonons in a periodically inverted polar superlattice," Phys. Rev. B **70**, 085319 (2004).